

DOI:10.1002/ejic.201500739

Bis(quinoxaline-dithiolato)nickel(III) Complexes [Bu₄N][Ni^{III}(6,7-qdt)₂] and [Ph₄P][Ni^{III}(Ph₂6,7-qdt)₂] ·CHCl₃ (6,7-qdt = Quinoxaline-6,7-dithiolate; Ph₂6,7-qdt = Diphenylquinoxaline-6,7-dithiolate): Synthesis, Spectroscopy, Electrochemistry, DFT Calculations, Crystal Structures and Hirshfeld Surface Analysis

Indravath Krishna Naik,^[a] Rudraditya Sarkar,^[a] and
Samar K. Das*^[a]

Keywords: Nickel / UV/Vis spectroscopy / Electrochemistry / Crystal structures / Supramolecular chemistry / ESR spectroscopy / Density functional calculations

Two bis(quinoxaline-dithiolato)nickel(III) complexes [Bu₄N][Ni^{III}(6,7-qdt)₂] (**1**; 6,7-qdt = quinoxaline-6,7-dithiolate) and [Ph₄P][Ni^{III}(Ph₂6,7-qdt)₂]·CHCl₃ (**2**; Ph₂6,7-qdt = diphenylquinoxaline-6,7-dithiolate) have been synthesized from their Ni^{II} analogues by iodine oxidation. Compounds **1** and **2** have been characterized by routine spectral analysis and single-crystal X-ray structure determination. Nickel(III) complexes **1** and **2** exhibit redshifted absorption bands compared with their Ni^{II} analogues; the electronic absorption spectral studies have been corroborated by DFT calculations. Electro-

chemical studies on **1** and **2** are consistent with those of their Ni^{II} analogues. Electron spin resonance (ESR) studies confirm that nickel is present in both **1** and **2** in its +3 oxidation state. This is also consistent with the fact that only one cation (Bu₄N⁺ for **1** and Ph₄P⁺ for **2**) is present in the respective crystal structures. The crystal structures of both compounds are characterized by C–H···S and C–H···N hydrogen-bonding interactions. Hirshfeld surface analyses have been studied to gain deep insight into the hydrogen-bonding interactions around/among the coordination complex anions.

Introduction

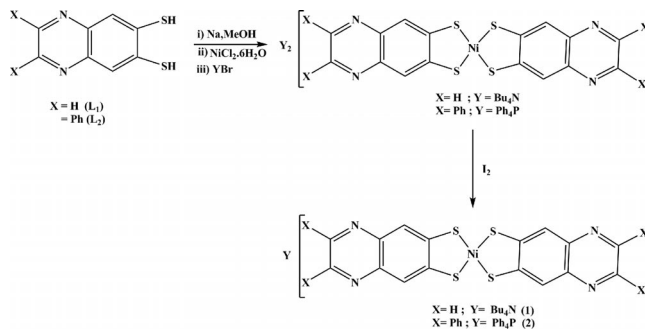
Metal–dithiolene complexes have been of considerable interest to synthetic inorganic chemists for more than four decades. In recent years, the design and synthesis of metal–bis(dithiolene) complexes have drawn great attention because of their potential applications as conducting and magnetic,^[1] nonlinear optical materials^[2] and near-infrared (NIR) dyes.^[3] Square-planar bis(dithiolene) metal coordination complexes are generally characterized by a high degree of delocalization within the chelate ring involving the metal ion, which contributes considerably to the low-energy electronic transition between the HOMO and the LUMO.^[4] This large delocalization is responsible for metal–dithiolene complexes showing absorption bands in the near-infrared (NIR) region. In the last few years, we and others have been working on transition-metal–dithiolene coordination complexes from the perspective of supramolecular chemistry^[5]

as well as bioinorganic chemistry.^[6] Recently, we reported on the influence of substituents of the coordinated dithiolato ligands on the electronic and electrochemical properties of a new square-planar nickel(II)–bis(quinoxaline-6,7-dithiolate) system.^[7] These ligands, because of their non-innocent behaviour, can stabilize coordination complexes in several oxidation states of the pertinent metal.^[4] Generally, the dianionic state (M^{II} oxidation state) is the most stable state for bis(dithiolene) complexes, but in some cases they can be isolated as monoanionic (M^{III} oxidation state) or even as neutral complexes (M^{IV} oxidation state). Ni^{III}–dithiolene complexes are of special interests because of their importance in the context of bioinorganic chemistry^[8] and catalysis.^[9] The bioinorganic aspect of nickel(III)–dithiolene complexes is related to the modelling of the active sites of [NiFe]H₂ase, for which extended X-ray absorption fine structure (EXAFS)/electron paramagnetic resonance (EPR) studies indicate that the formal oxidation state of the Ni centre in the resting state of the active site is paramagnetic Ni^{III}.^[8] The catalytic importance of Ni^{III} coordination complexes can be recognized by the fact that recently nickel(III) complexes have been employed as catalysts in C–C and C–heteroatom bond-formation reactions.^[9] This prompted us to explore Ni^{III} coordination complexes. The present

[a] School of Chemistry, University of Hyderabad,
P. O. Central University, Hyderabad 500046, India
E-mail: skdas@uohyd.ac.in
samar439@gmail.com
http://chemistry.uohyd.ac.in/~skd/

Supporting information for this article is available on the WWW under <http://dx.doi.org/10.1002/ejic.201500739>.

work deals with two nickel(III)–dithiolene complexes $[\text{Bu}_4\text{N}][\text{Ni}(\text{6,7-} \text{qdt})_2]$ (**1**; 6,7-qdt = quinoxaline-6,7-dithiolate) and $[\text{Ph}_4\text{P}][\text{Ni}(\text{Ph}_2\text{6,7-} \text{qdt})_2] \cdot \text{CHCl}_3$ (**2**; $\text{Ph}_2\text{6,7-} \text{qdt}$ = diphenylquinoxaline-6,7-dithiolate). We have chosen a phenyl group as a substituent attached to the aromatic ring in compound **2** to investigate the influence of the phenyl substituent on the electronic and electrochemical properties of a bis(dithiolate) Ni^{III} square-planar coordination complex (for example, compound **2**) with respect to an unsubstituted one (compound **1**). We describe here the synthesis, crystal structures, spectroscopy and electrochemistry of compounds **1** and **2**, including DFT calculations and Hirshfeld surface analyses of the complex anions.



Scheme 2. Synthesis of Ni^{III} -bis(6,7-quinoxaline-dithiolate) compounds **1** and **2**.

Results and Discussion

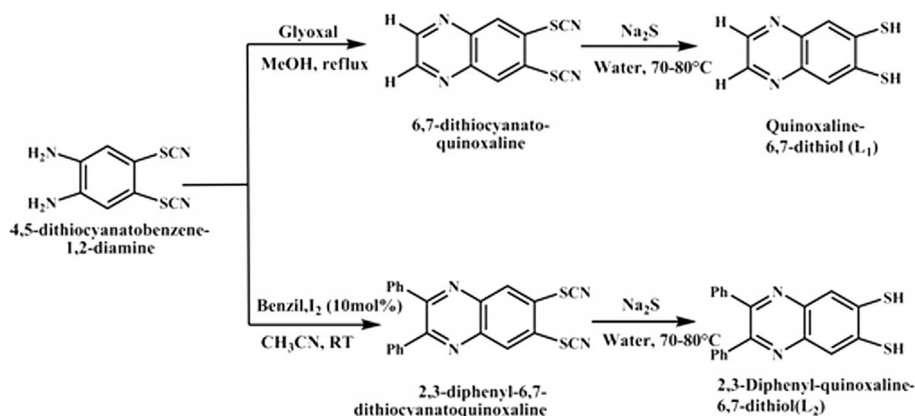
Synthesis and General Characterization

The synthetic route for the synthesis of the two dithiolate ligands used in this study (L_1 and L_2) is shown in Scheme 1. The synthesis of the corresponding Ni^{II} –(bis)dithiolate complexes $[\text{Bu}_4\text{N}]_2[\text{Ni}^{\text{II}}(\text{6,7-} \text{qdt})_2]$ and $[\text{Ph}_4\text{P}]_2[\text{Ni}^{\text{II}}(\text{Ph}_2\text{6,7-} \text{qdt})_2]$ was performed by a procedure reported earlier and shown in Scheme 2.^[7] The electrochemical studies of these two Ni^{II} compounds demonstrate that they can be oxidized at a low potential to the corresponding one-electron oxidized compounds $[\text{Bu}_4\text{N}][\text{Ni}^{\text{III}}(\text{6,7-} \text{qdt})_2]$ (**1**) and $[\text{Ph}_4\text{P}][\text{Ni}^{\text{III}}(\text{Ph}_2\text{6,7-} \text{qdt})_2] \cdot \text{CHCl}_3$ (**2**). Accordingly, we synthesized compounds **1** and **2** by chemical oxidation of $[\text{Bu}_4\text{N}]_2[\text{Ni}^{\text{II}}(\text{6,7-} \text{qdt})_2]$ and $[\text{Ph}_4\text{P}]_2[\text{Ni}^{\text{II}}(\text{Ph}_2\text{6,7-} \text{qdt})_2]$, respectively, by using iodine as shown in Scheme 2.

UV/Vis/NIR Spectra

The UV/Vis/NIR spectra of compound **1** and its parent compound $[\text{Bu}_4\text{N}]_2[\text{Ni}^{\text{II}}(\text{6,7-} \text{qdt})_2]$ are shown in part a of Figure 1. The electronic spectra of compound **2** and its corresponding parent compound $[\text{Ph}_4\text{P}]_2[\text{Ni}^{\text{II}}(\text{Ph}_2\text{6,7-} \text{qdt})_2]$ in DMF solutions are shown in part b of Figure 1. In our

earlier report, we assigned the absorption bands at 619 and 662 nm for the parent Ni^{II} compounds $[\text{Bu}_4\text{N}]_2[\text{Ni}^{\text{II}}(\text{6,7-} \text{qdt})_2]$ and $[\text{Ph}_4\text{P}]_2[\text{Ni}^{\text{II}}(\text{Ph}_2\text{6,7-} \text{qdt})_2]$, respectively, in DMF solutions to mixed-metal-ligand-to-ligand charge-transfer transitions based on DFT calculations because relevant the HOMOs include mixed metal-ligand-based orbitals and the LUMOs were defined as ligand-based π -MOs.^[7] Careful analysis of these spectra reveals the appearance of weak features beyond 800 nm, which were explained by the presence of oxidized impurities (corresponding to Ni^{III} complexes), formed by oxidation with air of $[\text{Bu}_4\text{N}]_2[\text{Ni}^{\text{II}}(\text{6,7-} \text{qdt})_2]$ and $[\text{Ph}_4\text{P}]_2[\text{Ni}^{\text{II}}(\text{Ph}_2\text{6,7-} \text{qdt})_2]$, which have very low oxidation potentials. Thus, when we oxidize these two Ni^{II} complexes $[\text{Bu}_4\text{N}]_2[\text{Ni}^{\text{II}}(\text{6,7-} \text{qdt})_2]$ and $[\text{Ph}_4\text{P}]_2[\text{Ni}^{\text{II}}(\text{Ph}_2\text{6,7-} \text{qdt})_2]$ chemically by iodine and isolated the compounds $[\text{Bu}_4\text{N}][\text{Ni}(\text{6,7-} \text{qdt})_2]$ (**1**) and $[\text{Ph}_4\text{P}][\text{Ni}(\text{Ph}_2\text{6,7-} \text{qdt})_2] \cdot \text{CHCl}_3$ (**2**), we observe that the absorption bands at 619 and 662 nm for compounds $[\text{Bu}_4\text{N}]_2[\text{Ni}^{\text{II}}(\text{6,7-} \text{qdt})_2]$ and $[\text{Ph}_4\text{P}]_2[\text{Ni}^{\text{II}}(\text{Ph}_2\text{6,7-} \text{qdt})_2]$, respectively, disappear. At the same time, broad bands at approximately 853 nm ($\epsilon = 16320 \text{ L mol}^{-1} \text{ cm}^{-1}$) and approximately 530 nm ($\epsilon = 14280 \text{ L mol}^{-1} \text{ cm}^{-1}$) appear for compound **1** as shown in Figure 1 (a). Similarly for compound **2**, absorption bands appear at approximately 880 nm ($\epsilon = 8160 \text{ L mol}^{-1} \text{ cm}^{-1}$) and approximately 554 nm ($\epsilon = 12440 \text{ L mol}^{-1} \text{ cm}^{-1}$) as shown in Figure 1 (b).



Scheme 1. Synthesis of quinoxaline dithiolate ligands L_1 and L_2 .

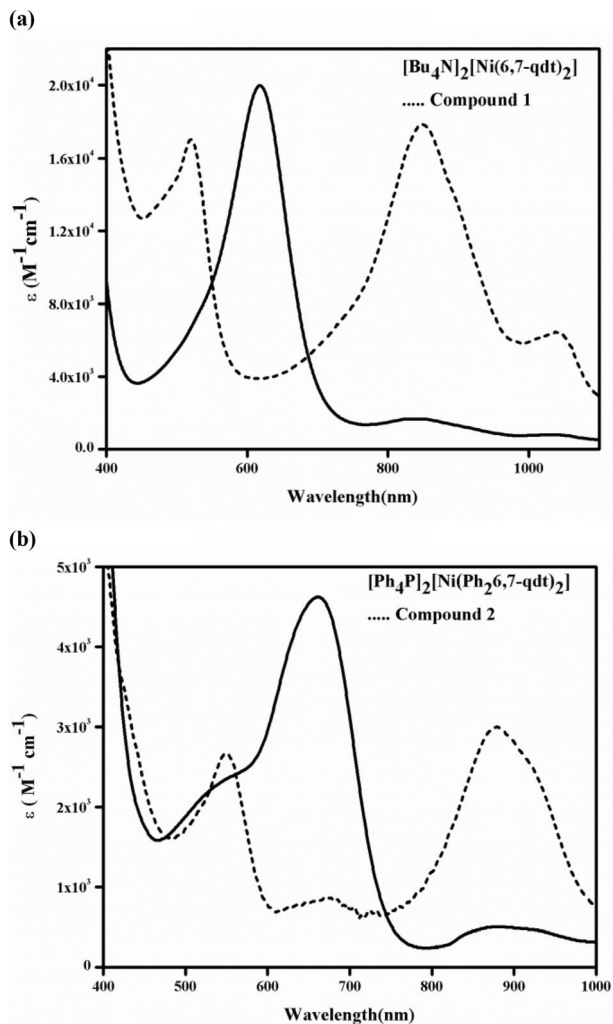


Figure 1. (a) UV/Vis/NIR spectra of compound **1** (3.42×10^{-5} M) and corresponding parent compound $[\text{Bu}_4\text{N}]_2[\text{Ni}(6,7\text{-qdt})_2]$ (4.64×10^{-5} M) in DMF solutions. (b) UV/Vis-NIR spectra of compound **2** (5.4×10^{-5} M) and corresponding parent compound $[\text{Ph}_4\text{P}]_2[\text{Ni}(\text{Ph}_2,6,7\text{-qdt})_2]$ (7.1×10^{-5} M) in DMF solutions.

DFT Calculations

We performed ground-state electronic structure calculations for mono anions of compounds **1** and **2** by using density functional theory (DFT; see computational details in the Experimental Section), as implemented in the Gaussian 09 program.^[10] Owing to the odd number of total electrons (Ni^{III} ion, d^7 system), we found singly occupied α -spin HOMOs for both complex anions; at the same time, the comparable β -spin MO is vacant. The molecular orbital diagrams of the HOMOs and LUMOs of compounds **1** and **2** are given in the Supporting Information (Figures S8 and S9). Experimentally, we observed an absorption band for $[\text{Bu}_4\text{N}][\text{Ni}(6,7\text{-qdt})_2]$ (**1**) at 1060 nm. From the theoretical vertical excitation, determined by the time-dependent (TD) DFT method, this low-energy absorption band corresponds to the transition from β -spin HOMO to β -spin LUMO transition, (Figure 2, A); the theoretical value of this band is approximately 1272 nm as shown in Figure 2 (A). The

low intensity of this band (Figure 1 (a), dotted line) is explained by its low oscillator strength (f value) of 0.0172. The second high-intensity absorption band observed for compound **1** appeared at 853 nm (Figure 1 (a), dotted line), which can theoretically be attributed to the β -spin HOMO–2 to β -spin LUMO transition as shown in Figure 2 (B). The theoretical value of this band is approximately 985 nm with a high oscillator strength of 0.2841. This transition at 853 nm (compound **1**) also contains a contribution from the transition from α -spin HOMO–6 to α -spin LUMO (Figure 1, C). The former transition (β -spin HOMO–2 to β -spin LUMO) has maximum 88% impact on the total absorption and the latter transition (α -spin HOMO–6 to α -spin LUMO, Figure 1, C) has a 12% contribution to the total absorption at 853 nm (theoretical value 985 nm). The third experimental absorption band of compound **1**, which appears at 530 nm (Figure 1 (a), dotted line), cannot be explained properly by DFT calculations, because the corresponding theoretical value (553 nm) is characterized by a poor oscillator strength (0.0001), even though the observed absorption (at 530 nm) is an intense band. The nickel ion does not have any significant role in the low-energy absorption at 1060 nm (Figure 1 (a), dotted line) of compound **1** (theoretical value 1272 nm) as shown in Figure 2 (A). Conversely, for the highly intense observed band at 853 nm (theoretical value 985 nm), the central metal (nickel) ion plays a crucial role (Figure 2, B and C). As shown in Figure 2 (B), β -spin HOMO–2 is of π -type character and β -spin LUMO is of π^* -type character. We also find a contribution from the central metal (nickel) in the HOMOs (both HOMO–2 and HOMO–6) and high electron density in the π^* orbitals of dithiolate ligands in the LUMOs. As both the HOMOs (Figure 2, B and C) include mixed-metal-ligand-based orbitals, we can say that the major transition (853 nm) is a “mixed-metal-ligand-to-ligand” (MMLL) charge-transfer transition.^[7] Although the oxidation state of nickel in compound **1** is formally +3 (confirmed from ESR spectroscopy and electrochemical studies), electron density corresponds to the $3p_y$ atomic orbital (AO) of nickel is situated at the nickel centre in the β -spin HOMO–2 MO. All $3p_y$ AOs of the surrounding four sulfur donor atoms (all sulfur atoms have positive MO coefficients) and the central nickel $3p_y$ AO form a linear combination to create the π -bonding-type β -spin HOMO–2 (Figure 2, B). Owing to the participation of both ligand (sulfur donor) and metal (nickel) AOs, the present calculated HOMO is described as a mixed-metal-ligand-type of MO. In the case of the π^* -type β -spin LUMO, the same AOs of sulfur (two sulfur atoms have positive MO coefficients and the other two sulfur atoms have negative MO coefficients) form the anti-bonding-type MO, where no contribution from the nickel atom is found. Thus, this LUMO is characterized only by ligand AOs. As a result, the overall transition, shown in Figure 2 (B), can be depicted as a “mixed-metal-ligand-to-ligand” transition.

Next, we concentrated our focus on $[\text{Ph}_4\text{P}][\text{Ni}(\text{Ph}_2,6,7\text{-qdt})_2]$ (**2**). A noticeable redshift of the most intense peak is observed in case of compound **2** compared with that of

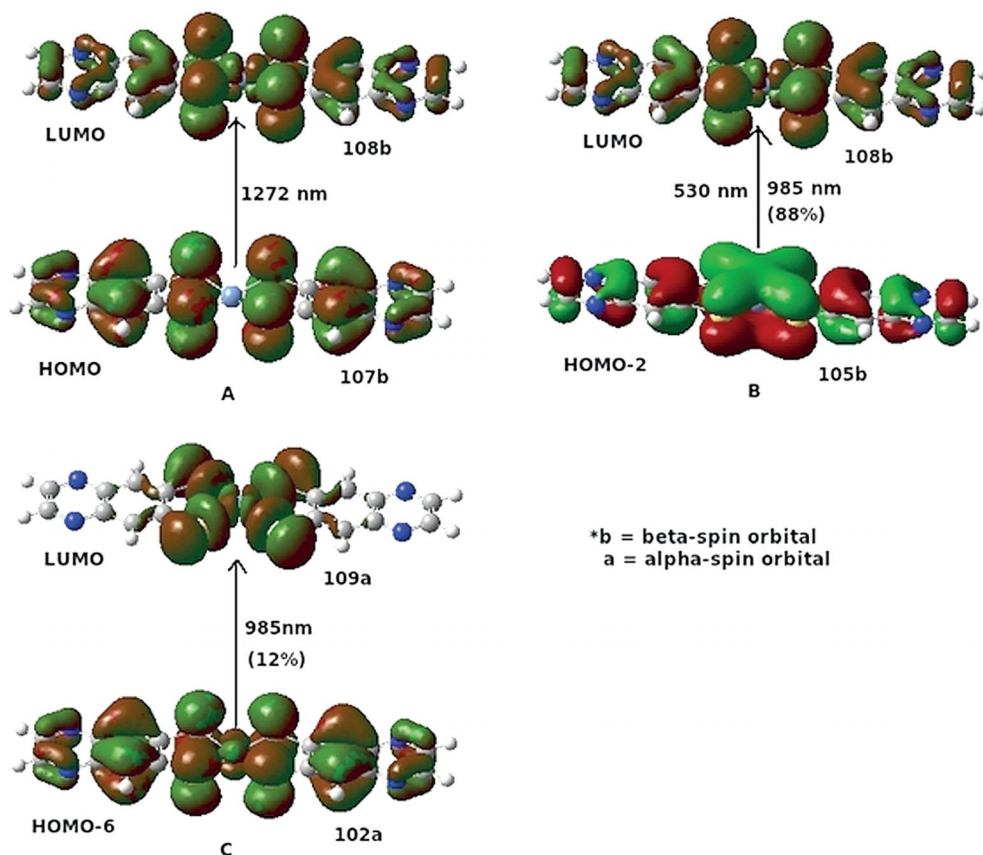


Figure 2. HOMO and LUMO diagrams originating from molecular orbital calculations for the mono anion of compound 1.

[Bu₄N][Ni(6,7-qdt)₂] (**1**). Experimentally, the most intense absorption band is observed at 880 nm for compound **2**, which is 30 nm from the most intense peak of compound **1**. The theoretical value of this observed band at 880 nm is 1071 nm with an *f* value of 0.4736. This theoretical peak is attributed mainly to the transition from β -spin HOMO–3 to β -spin LUMO (Figure 3, A), which contributes 80% to the total observed absorption band at 880 nm. The rest of the contribution arises from β -spin HOMO–5 to β -spin LUMO (11%, Figure 3, B) and α -spin HOMO–7 to α -spin LUMO (9%, Figure 3, C) transitions. The other major absorption of compound **2**, for which the observed (554 nm) as well as theoretical (553 nm) values are almost identical, is attributed to the transition from β -spin HOMO–5 to β -spin LUMO, which contributes 54% to the total absorption at 554 nm (Figure 3, B), and also takes part in the absorption at 880 nm as mentioned earlier. As shown in Figure 3, A and C, it is clear that the maximum electron density cloud is situated around the central metal ion, nickel, which indicates that central metal ion has considerable contribution to the electronic absorption at 880 nm (compound **2**). Lateral overlap in HOMO–3 (Figure 3, A) indicates that it has a π -bonding nature (mixed-metal-ligand π orbitals), whereas the corresponding LUMO is ligand-based and π^* in nature. Therefore, in the case of compound **2**, the major absorption at 880 nm can be assigned to “mixed-metal-ligand-to-ligand” (MMLL) charge-transfer transitions.^[7] As observed in compound **1**, a similar scenario of linear com-

bination of AOs is also observed in the case of compound **2**, where the 3p_z AOs of both nickel and sulfur are the participating orbitals.

It has already been mentioned that the most intense absorption band is observed at 880 nm for [Ph₄P][Ni(Ph₂6,7-qdt)₂] \cdot CHCl₃ (**2**), which is around 30 nm redshifted from the most intense peak (853 nm) of [Bu₄N][Ni(6,7-qdt)₂] (**1**). As we go from compound **1** to compound **2**, two phenyl groups per ligand are added as substituents, replacing two protons (Scheme 2). Particular substituents on an aromatic system can lead to mesomeric as well as inductive effects. The mesomeric effect arises from the delocalization of π -electrons between the substituent and aromatic core. On the other hand, the inductive effect is fully associated with the σ -electron system of the aromatic ring. In the case of [Ph₄P][Ni(Ph₂6,7-qdt)₂] \cdot CHCl₃ (**2**), both mesomeric and inductive effects are to be considered. This is because the substituted phenyl group (compound **2**) can be involved in both these effects. The inductive effect can be initiated by an electron-withdrawing substituent or by an electron-donating substituent. In the present study (compound **2**), the phenyl substituent acts as an electron-withdrawing group, which can be established from the following discussion. An electron-withdrawing group pulls the σ -electron density from the ligand by the inductive effect; thereby, reducing the repulsive Coulombic interactions between the electrons occupying the ligand-localized π -MOs and the electrons of the σ -system. Thus, an electron-withdrawing substituent in the

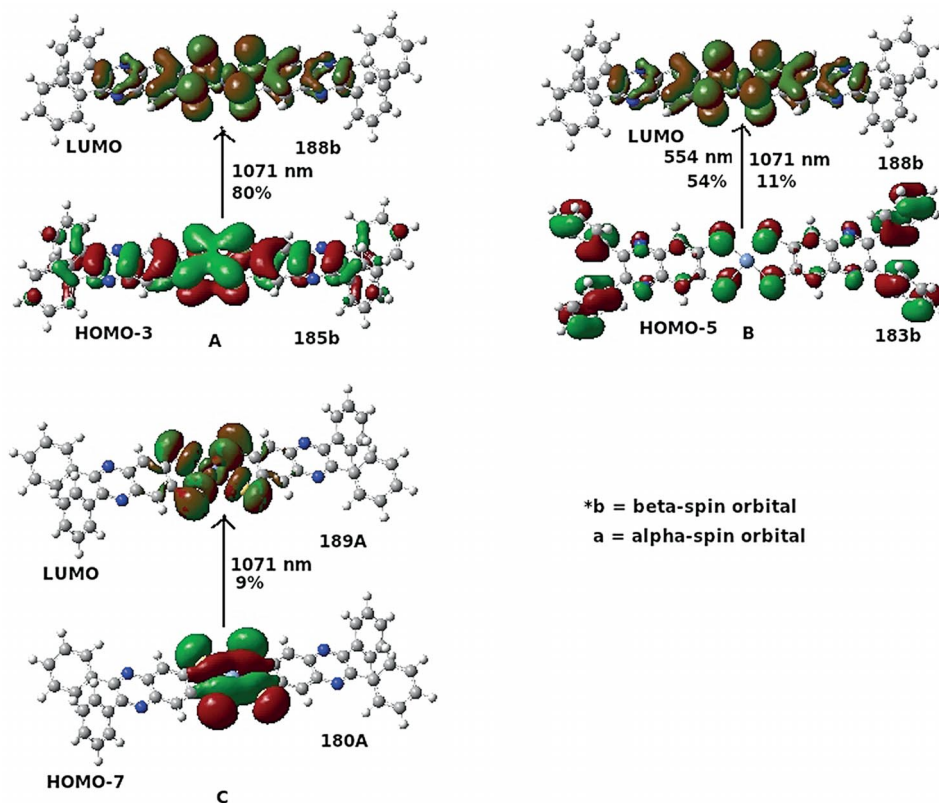


Figure 3. HOMO and LUMO diagrams originating from molecular orbital calculations for the mono anion of compound **2**.

present system causes a lowering of the energy of the LUMOs (because these are purely π -MO of the dithiolate ligand, Figures 1 and 2) without lowering the energy of the HOMOs significantly (because they are a mixture of nickel d-orbital character and dithiolate π -type orbitals). This should cause a redshift in the relevant electron absorption spectra (the energy gap between HOMO and LUMO would essentially be decreased). Conversely, an electron-releasing substituent in the present system would cause a blueshift in the electronic absorption spectra because the energy gap between the HOMO and LUMO would essentially be increased (an electron-donating group increases the electron density toward the dithiolate ligand and thereby increases the repulsive Coulombic interactions between the ligand centred π -MOs and σ -electrons). Therefore, in the case of compound **2**, the substituent phenyl group acts as an electron-withdrawing group and causes the redshift of 30 nm in the pertinent electron absorption spectra when we go from compound **1** (no substituent) to compound **2** (phenyl group as a substituent).

In the case of the mesomeric effect, the substituent phenyl group (compound **2**) can share its π -electrons with the aromatic core associated with the dithiolato ligand by resonance. The prevalence of mesomeric effects in the present system is supported by DFT calculations. When we compare parts A and C in Figure 3 with parts B and C in Figure 2, we find relatively more electron density at the central metal ion in compound **2** (where the phenyl substituent exerts a mesomeric effect by resonance) in comparison to

that at the central metal ion in compound **1** (where there is no substituent in place of hydrogen). The higher electron density at the central metal ion makes electronic transitions easier in the case of compound **2**, which probably causes the redshift of the more intense band compared with compound **1**. Thus, both inductive and mesomeric effects are responsible for this redshift, which is consistent with DFT calculations.

As shown in Figure 1 (a and b), the major electron absorption bands for Ni^{III} complexes (compounds **1** and **2**) appear in redshifted regions compared with their parent Ni^{II} analogues [Bu₄N]₂[Ni^{II}(6,7-qdt)₂] and [Ph₄P]₂[Ni^{II}(Ph₂6,7-qdt)₂]. Compounds **1** and **2** are one-electron oxidized products of their Ni^{II} parent compounds [Bu₄N]₂[Ni^{II}(6,7-qdt)₂] and [Ph₄P]₂[Ni^{II}(Ph₂6,7-qdt)₂]. When compound [Bu₄N]₂[Ni^{II}(6,7-qdt)₂] is oxidized by iodine to its Ni^{III} analogue (compound **1**), the electronic absorption band at 619 nm (parent Ni^{II} compound) shifts to 853 nm (compound **1**). Similarly, when compound [Ph₄P]₂[Ni^{II}(Ph₂6,7-qdt)₂] is oxidized by iodine to its Ni^{III} form (compound **2**), the major electronic absorption band at 662 nm (parent Ni^{II} compound) moves to 880 nm (compound **2**).

This large redshift (234 nm for compound **1** and 218 nm for compound **2**) of the major electronic absorption bands on going from Ni^{II} to Ni^{III} complexes can be attributed to the central metal ion, nickel, which, in its +3 oxidation state, pulls the σ -electron density from the coordinated dithiolate ligand and reduces the repulsion-type Coulombic interactions between the electrons in the σ -system and elec-

trons occupying the ligand-localized π -MOs. This causes the lowering of the energy of the LUMOs (purely π -MOs of the dithiolate ligand, see Figures 2 and 3) without lowering the energy of the HOMOs (mixed-metal-ligand π orbitals, Figures 2 and 3), resulting in the decrease in the energy gap between the HOMO and LUMO. This explains the large redshift in the electronic absorption maxima when the Ni^{II} complex is oxidized to its Ni^{III} analogue. Theoretically simulated absorption spectra for the Ni^{III} complex anions of **1** and **2** are displayed in the Supporting Information (Figures S10 and S11).

Electron Spin Resonance (ESR) Spectra

The ESR spectra of solid samples of $[\text{Bu}_4\text{N}][\text{Ni}^{\text{III}}(6,7\text{-qdt})_2]$ (**1**) and $[\text{Ph}_4\text{P}][\text{Ni}^{\text{III}}(\text{Ph}_26,7\text{-qdt})_2]\cdot\text{CHCl}_3$ (**2**) were recorded at room temperature and 123 K. The ESR spectra recorded at 123 K are presented in Figure 4. Compound **1** exhibits a rhombic-type signal: $g_x = 2.246$, $g_y = 2.156$ and $g_z = 2.065$. However, compound **2** shows an axial signal with $g_{\perp} > g_{\parallel}$: $g_{\perp} = 2.133$ and $g_{\parallel} = 2.049$. This is consistent with low-spin Ni^{III} (d^7 , $S = 1/2$) in a tetragonal geometry ($g_{\perp} > g_{\parallel}$) with one unpaired electron in the d_{z^2} orbital.^[11] The anisotropy in the ESR spectra implies some contribution from the d orbital of nickel to the total spin density, which is consistent with DFT calculations (see above). The ESR data suggest that the unpaired electrons in compounds **1** and **2** are not localized on the ligands because the ESR spectra do not show any sharp signal near $g = 2.003$ (an organic ligand radical usually shows a sharp signal at $g = 2.003$). The present ESR data and their comparison with those of already known mononuclear Ni^{III} square-planar complexes^[11] confirm that compounds **1** and **2** are formally Ni^{III} complexes. The rhombic ESR feature (compound **1**) is not unusual for a square-planar Ni^{III} complex because of distortion from the square-planar geometry. However, compound **2** exhibits an axial feature in its ESR spectrum, even though both complexes are square planar. It can be speculated that the presence of a solvent molecule (CHCl_3) in the

crystal lattice of compound **2** might have made this difference. A square-planar bis(dithiolato)- Ni^{III} complex showing an axial ESR feature is known.^[12]

Electrochemistry

We mentioned in our earlier report^[7] that the parent compounds $[\text{Bu}_4\text{N}]_2[\text{Ni}^{\text{II}}(6,7\text{-qdt})_2]$ and $[\text{Ph}_4\text{P}]_2[\text{Ni}^{\text{II}}(\text{Ph}_26,7\text{-qdt})_2]$ of the present Ni^{III} compounds $[\text{Bu}_4\text{N}][\text{Ni}^{\text{III}}(6,7\text{-qdt})_2]$ (**1**) and $[\text{Ph}_4\text{P}][\text{Ni}^{\text{III}}(\text{Ph}_26,7\text{-qdt})_2]\cdot\text{CHCl}_3$ (**2**) undergo reversible oxidation at very low oxidation potentials in MeOH solutions: $[\text{Bu}_4\text{N}]_2[\text{Ni}^{\text{II}}(6,7\text{-qdt})_2]$ undergoes oxidation at $E_{1/2} = +0.12$ V versus Ag/AgCl ($\Delta E = 74$ mV), corresponding to the $[\text{Ni}^{\text{III}}(6,7\text{-qdt})_2]^{1-}/[\text{Ni}^{\text{II}}(6,7\text{-qdt})_2]^{2-}$ redox couple, and $[\text{Ph}_4\text{P}]_2[\text{Ni}^{\text{II}}(\text{Ph}_26,7\text{-qdt})_2]$ undergoes oxidation at $E_{1/2} = +0.033$ V versus Ag/AgCl ($\Delta E = 65$ mV), corresponding to the $[\text{Ni}^{\text{III}}(\text{Ph}_26,7\text{-qdt})_2]^{1-}/[\text{Ni}^{\text{II}}(\text{Ph}_26,7\text{-qdt})_2]^{2-}$ couple. In the present study, we could not perform electrochemical studies in MeOH owing to low solubility. Compounds **1** and **2** are not freely soluble in MeOH. We, thus, performed the cyclic voltammetric studies of compounds **1** and **2** in DMF solutions, each containing 0.10 M $[\text{Bu}_4\text{N}]\text{ClO}_4$ as the supporting electrolyte. As shown in Figure 5, cyclic voltammograms of compounds **1** and **2** exhibit quasi-reversible reductive responses at $E_{1/2} = +0.225$ V versus Ag/AgCl ($\Delta E = 87$ mV) and $E_{1/2} = +0.044$ V versus Ag/AgCl ($\Delta E = 82$ mV), respectively. Based on the $E_{1/2}$ values of the oxidative responses of the Ni^{II} analogues $[\text{Bu}_4\text{N}]_2[\text{Ni}^{\text{II}}(6,7\text{-qdt})_2]$ and $[\text{Ph}_4\text{P}]_2[\text{Ni}^{\text{II}}(\text{Ph}_26,7\text{-qdt})_2]$ in MeOH^[7] as well as in DMF (see the Supporting Information), we can assign these reductive responses of compounds **1** and **2** to the $[\text{Ni}^{\text{III}}(6,7\text{-qdt})_2]^{1-}/[\text{Ni}^{\text{II}}(6,7\text{-qdt})_2]^{2-}$ and $[\text{Ni}^{\text{III}}(\text{Ph}_26,7\text{-qdt})_2]^{1-}/[\text{Ni}^{\text{II}}(\text{Ph}_26,7\text{-qdt})_2]^{2-}$ couples, respectively.

The lower reduction potential value (+0.044 V) for the $[\text{Ni}^{\text{III}}(\text{Ph}_26,7\text{-qdt})_2]^{1-}/[\text{Ni}^{\text{II}}(\text{Ph}_26,7\text{-qdt})_2]^{2-}$ couple (compound **2**) compared with that for the $[\text{Ni}^{\text{III}}(6,7\text{-qdt})_2]^{1-}/[\text{Ni}^{\text{II}}(6,7\text{-qdt})_2]^{2-}$ couple (compound **1**; +0.225 V) can be explained by the inductive effect of the phenyl substituents, which pull electrons from the metal–dithiolate chelate and,

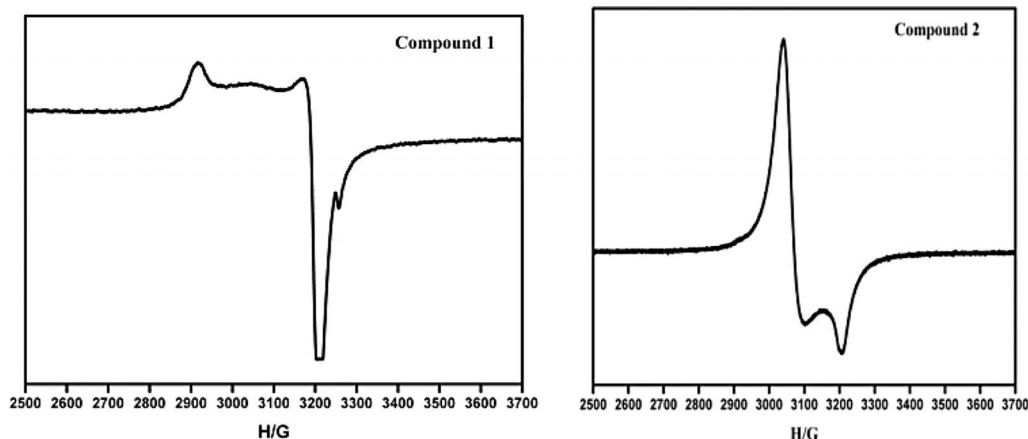


Figure 4. Electron spin resonance spectra of the compounds **1** (left) and **2** (right) in their powder form at 123 K.

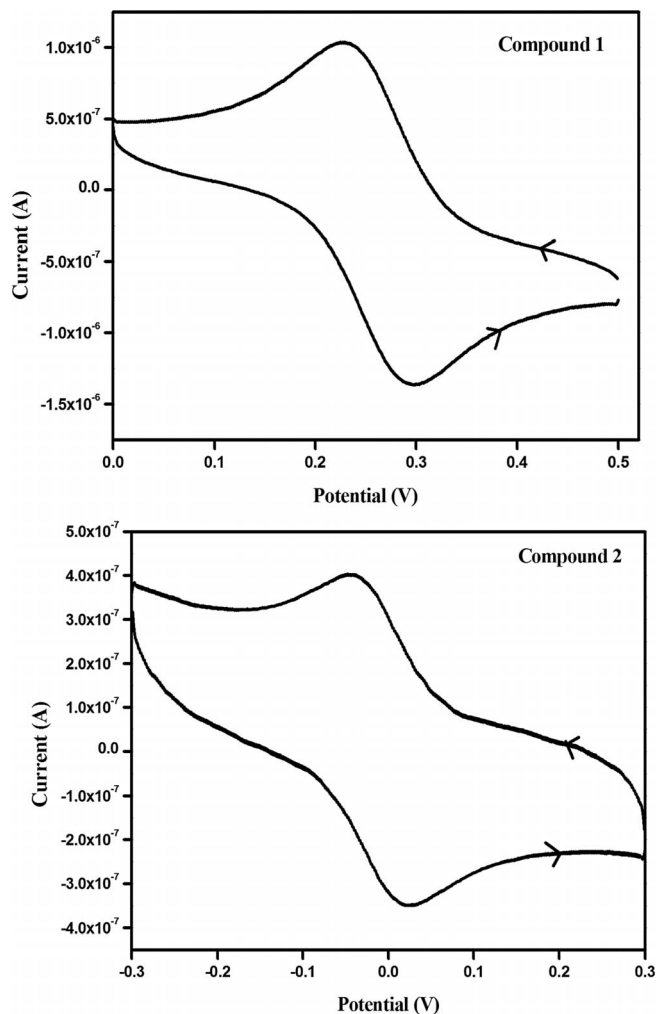


Figure 5. Cyclic voltammograms of compounds **1** (top) and **2** (bottom) in DMF solution. Scan rate=0.01 mV s⁻¹, V vs. Ag/AgCl.

thus, the relevant metal centre would be more easily reduced. The low reduction potential value of compound **2** compared with that of compound **1** can also be justified from the perspective of theoretical calculations, which show that the energy gap between the HOMO and LUMO is less in the case of compound **2** compared with that of compound **1**. In both cases (compounds **1** and **2**), the lowest unoccupied orbital is the β -spin LUMO (see above). If the system is reduced by one electron, the electron has to occupy the β -spin LUMO, which is more stabilized in the case of compound **2** (HOMO–LUMO gap is smaller). Thus, compound **2** would be reduced more easily (+0.044 V) than compound **1** (+0.225 V).

ESR spectroscopy (see above) and single-crystal X-ray crystallography (see below) indicate that the isolated compounds **1** and **2** have nickel in its +3 oxidation state. Keeping this in mind, during the cyclic voltammetric experiments, we took the first scans starting from the positive side (+0.5 V for compound **1** and +0.3 V for compound **2**) and we found first reduction followed by oxidation in the respective cyclic voltammograms (shown by arrows, Figure 5). Thus, the electrochemical experiments clearly point

out that the oxidation state of nickel in the isolated compounds **1** and **2** is +3.

Description of Crystal Structures

[Bu₄N][Ni(6,7-qdt)₂] (**1**)

The crystals of compound **1** suitable for single-crystal X-ray structure determination were obtained from acetonitrile solution by the vapour diffusion of diethyl ether. Crystallographic analysis revealed that compound **1** crystallizes in a monoclinic system with space group $P2_1/c$. The relevant asymmetric unit contains two crystallographically independent halves of the [Ni(6,7-qdt)₂]¹⁻ molecule and one tetrabutylammonium cation. The thermal ellipsoid diagram of the asymmetric unit in the crystal structure of compound **1** is shown in Figure 6 (a). The relevant molecular packing diagram is shown in Figure 6 (b). The basic crystallographic data for compound **1** are presented in Table 1 and selected bond angles and interatomic distances are described in Table 2. The geometry around nickel ion in both the crystallographically independent complexes is roughly square planar, consisting of four sulfur donor atoms from two 6,7-qdt²⁻ dithiolato ligands. The relevant coordination angles are in the range 87.77(3)–92.23(3)° (Table 2). In the five-membered chelate rings involving the nickel ion, the Ni–S, C–S and C=C bond lengths are in the range 2.1431(7)–

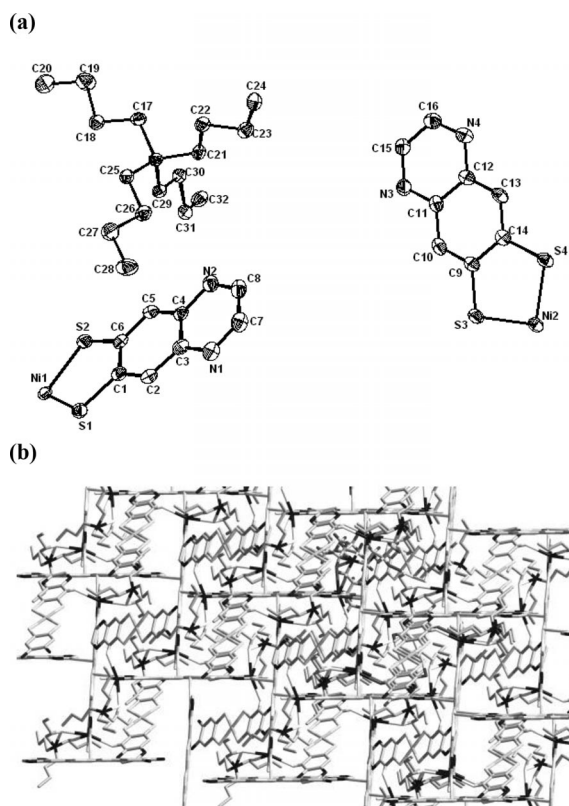


Figure 6. (a) Thermal ellipsoid plot (at the 50% probability level) of the asymmetric unit in the crystal structure of compound **1** (hydrogen atoms are omitted for clarity). (b) Molecular packing diagram for the crystal structure of compound **1**.

2.1555(7), 1.737(3)–1.746(3) and 1.423(4)–1.426(4) Å, respectively. The total charge of the Ni^{III} complex anion [Ni(6,7-qdt)₂]¹⁻ in compound [Bu₄N][Ni(6,7-qdt)₂] (**1**), unsurprisingly, –1, and this anionic charge is compensated by a [Bu₄N]⁺ cation as observed in the crystal structure (Figure 6).

Table 1. Crystal data and structural refinement parameters for compounds **1** and **2**.

	1	2
Empirical formula	C ₃₂ H ₄₄ N ₅ NiS ₄	C ₆₅ H ₄₅ Cl ₃ N ₄ NiPS ₄
Formula weight	685.67	1206.32
Temperature [K]	100(2)	100(2)
Crystal size [mm]	0.20 × 0.12 × 0.08	0.21 × 0.18 × 0.12
Crystal system	monoclinic	triclinic
Space group	<i>P</i> 2 ₁ / <i>c</i>	<i>P</i> $\bar{1}$
<i>Z</i>	4	2
Wavelength [Å]	0.71073	0.71073
<i>a</i> [Å]	13.8384(9)	13.294(10)
<i>b</i> [Å]	11.6926(8)	15.018(12)
<i>c</i> [Å]	22.4558(12)	15.677(12)
α [°]	90	70.818(12)
β [°]	113.333	80.368(12)
γ [°]	90	84.916(13)
Volume [Å ³]	3336.3(4)	2913
Calculated density [Mg m ⁻³]	1.365	1.375
Reflections collected/unique	33936/6533	10208/6861
<i>R</i> (int)	0.0548	0.13
<i>F</i> (000)	1452	1242
Max. and min. transmission	0.9342 and 0.8465	0.922 and 0.8693
θ range for data collection [°]	1.70–26.48	1.39–26.18
Refinement method	full-matrix least-squares on <i>F</i> ²	
Data/restraints/parameters	6533/0/386	10208/0/706
Goodness-of-fit on <i>F</i> ²	1.131	1.252
<i>R</i> ₁ / <i>wR</i> ₂ [<i>I</i> > 2 σ (<i>I</i>)]	0.0488/0.1029	0.1335/0.3135
<i>R</i> ₁ / <i>wR</i> ₂ (all data)	0.0576/0.1069	0.1719/0.3319
Largest diff. peak and hole [e Å ⁻³]	0.548 and –0.281	1.275 and –0.944

Table 2. Selected bond lengths [Å] and angles [°] for compounds **1** and **2**.

Compound 1 ^[a]			
Ni(1)–S(1)#1	2.1431(7)	Ni(1)–S(2)#1	2.1442(7)
Ni(2)–S(3)#2	2.1555(7)	Ni(2)–S(4)#2	2.1473(7)
S(1)#1–Ni(1)–S(1)	180.00(4)	S(1)–Ni(1)–S(2)	92.23(3)
S(1)#1–Ni(1)–S(2)	87.77(3)	S(4)–Ni(2)–S(3)	92.16(3)
S(4)–Ni(2)–S(3)#2	87.85(3)	S(3)–Ni(2)–S(3)#2	180.00(4)
C(1)–S(1)–Ni(1)	105.26(10)	C(6)–S(2)–Ni(1)	105.33(10)
C(9)–S(3)–Ni(2)	104.95(10)	C(14)–S(4)–Ni(2)	104.92(10)
Compound 2 ^[b]			
Ni(1)–S(3)	2.126(3)	Ni(1)–S(4)	2.129(3)
Ni(2)–S(1)	2.136(3)	Ni(2)–S(2)	2.134(3)
S(3)–Ni(1)–S(4)	92.03(12)	S(3)–Ni(1)–S(4)#1	87.97(12)
S(2)–Ni(2)–S(1)	92.17(11)	S(2)#2–Ni(2)–S(1)	87.83(11)
S(2)–Ni(2)–S(2)#2	180	S(1)#2–Ni(2)–S(1)	180.00(16)
S(3)–Ni(1)–S(3)#1	179.9(1)	S(4)–Ni(1)–S(4)#1	180.00(12)

[a] Symmetry transformations used to generate equivalent atoms: #1 –*x* + 2, –*y* + 2, –*z* + 1; #2 –*x* + 1, –*y* + 1, –*z* + 2. [b] #1 –*x* + 1, –*y*, –*z* + 1; #2 –*x* + 2, –*y* + 1, –*z* + 1.

To investigate the supramolecular structure, we looked at the C–H⋯S and C–H⋯N interactions in the crystal structure of compound **1**. We found that a supramolecular chain-like arrangement [Figure 7 (a)] is formed from anion–anion C–H⋯N interactions. On the other hand, inter-anion

C–H⋯S hydrogen-bonding interactions are responsible for the formation of a two-dimensional layer-like supramolecular arrangement [Figure 7 (b)]. In addition to inter-anionic supramolecular interactions, inter-cation–anion interactions exist (see the Supporting Information, Figure S5). Hydrogen-bonding parameters for the crystal structure of compound **1** are shown in Table 3.

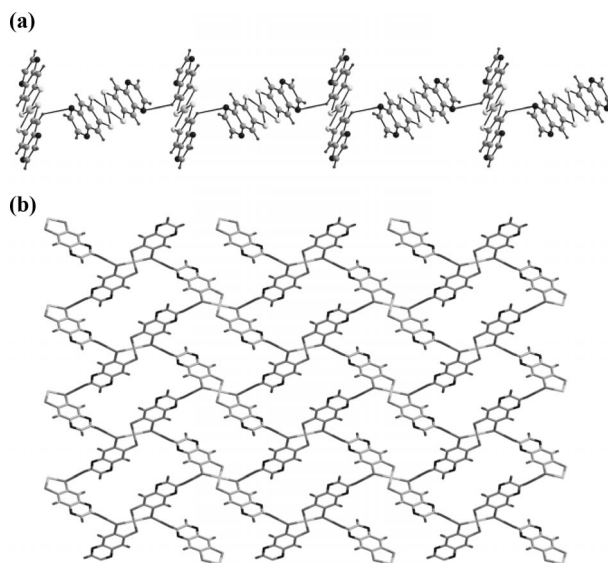


Figure 7. (a) Inter-molecular one dimensional supramolecular chain of [Ni(6,7-qdt)₂]¹⁻ formed by C–H⋯N weak interactions. (b) Two-dimensional supramolecular layer-like structure formed by inter-anion C–H⋯S weak interactions (viewed along the crystallographic *a*-axis).

Table 3. Hydrogen-bond parameters for compound **1**.^[a]

D–H⋯A	<i>d</i> (D–H) [Å]	<i>d</i> (H⋯A) [Å]	<i>d</i> (D⋯A) [Å]	<(DHA) ^[b] [°]
C(29)–H(29A)⋯N(2)	0.97	2.65	3.612(4)	172.9
C(26)–H(26B)⋯N(2)	0.97	2.70	3.603(4)	154.4
C(13)–H(13)⋯N(2)#3	0.93	2.67	3.390(4)	134.9
C(23)–H(23B)⋯S(3)#3	0.97	2.90	3.797(3)	154.7
C(7)–H(7)⋯S(1)#4	0.93	2.81	3.733(3)	169.6

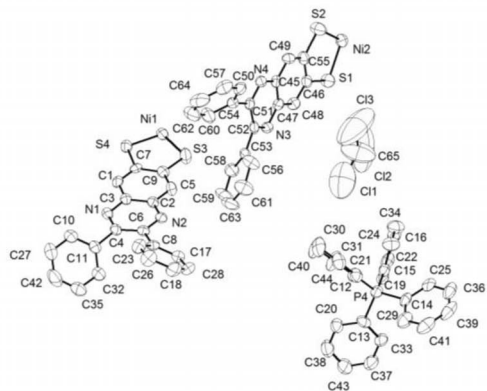
[a] Symmetry transformations used to generate equivalent atoms: #3 –*x* + 1, *y* – 1/2, –*z* + 3/2; #4 –*x* + 2, *y* – 1/2, –*z* + 3/2. [b] <(DHA): dihedral angle.

[Ph₄P][Ni(Ph₂6,7-qdt)₂]·CHCl₃ (**2**)

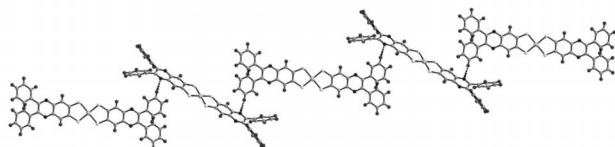
Crystals of [Ph₄P][Ni(Ph₂6,7-qdt)₂]·CHCl₃ (**2**) suitable for single-crystal X-ray structure determination were obtained from a CHCl₃ solution by vapour diffusion of diethyl ether. Compound **2** crystallizes in triclinic space group *P* $\bar{1}$. The asymmetric unit consists of two crystallographically independent halves of the [Ni(Ph₂6,7-qdt)₂]¹⁻ anion and one tetraphenylphosphonium cation along with a solvent molecule, as shown Figure 8 (a). The geometry around the Ni³⁺ ion, which is coordinated by four sulfur atoms from two Ph₂6,7-qdt²⁻ ligands, is a square-planar geometry with S1–N2–S2 and S3–Ni1–S4 coordination angles of 92.17(11) and 92.03(12), respectively, from two different crystallographically independent molecules. In the five-membered

coordinated chelate rings of both the crystallographically independent molecules, the Ni–S, C–S and C=C bond lengths are in the range 2.1431(7)–2.1555(7), 1.711(3)–1.740(3) and 1.407(4)–1.419(4) Å, respectively.

(a)



(b)



(c)

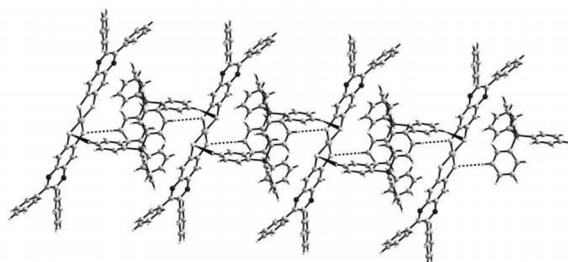


Figure 8. (a) Thermal ellipsoid diagram of compound **2** (at the 50% probability level), with hydrogen atoms omitted for clarity. (b) One-dimensional supramolecular chain-like arrangement formed by inter-anion interactions in the crystal structure of compound **2**. (c) Supramolecular chain-like structure formed by C–H...S weak interactions in compound **2**.

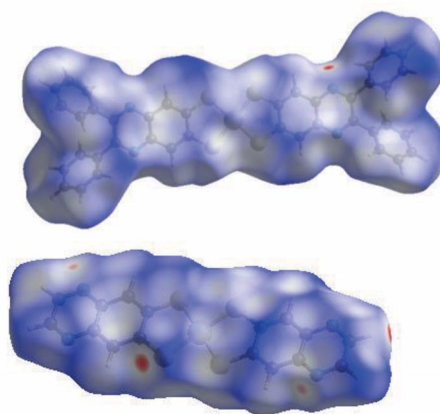
The crystal structure of compound **2** is also characterized by C–H...N and C–H...S supramolecular hydrogen-bonding interactions. The inter-anion C–H...N weak interactions lead to the formation of one-dimensional chain-like structure as shown in Figure 8 (b). On the other hand, the C–H...S hydrogen-bonding interactions between the complex anions and tetraphenylphosphonium cations lead to the construction of a sandwich-type extended arrangement as shown in Figure 8 (c).

Hirshfeld Surface Analysis

The hydrogen-bonding supramolecular interactions around the complex anions $[\text{Ni}^{\text{III}}(\text{6,7-qdt})_2]^{1-}$ and $[\text{Ni}^{\text{III}}(\text{Ph}_2\text{6,7-qdt})_2]^{1-}$ are further analysed with the Hirshfeld surfaces (HSs) and 2D fingerprint plots (FPs), which are generated by using the software Crystal explorer 3.1^[13] based on the CIF file. The 3D Hirshfeld surfaces offer additional

insight into the long- and short-range interactions experienced by the complex anions, and the 2D fingerprint plot, derived from the HSs, furnishes the nature, type and relative contribution of the intermolecular interactions. Generally, the directions and strengths of intermolecular interactions within the crystal are mapped onto the HSs by defining a descriptor “ d_{norm} ”, which is a ratio of the distance of any surface point to the nearest interior (d_i) and exterior (d_e) atom to the van der Waals radii (vdW) of the concerned atoms.^[14] Thus, when d_{norm} is negative, the sum of d_i and d_e , that is, the contact distance, is shorter than the sum of the relevant van der Waals radii, which is considered to be the closest contact and is visualized as red spots on the HSs as shown in Figure 9 (a). The white and blue colours indicate the contacts at vdW separation ($d_{\text{norm}} = 0$). The intermolecular contacts contained in Tables 3 and 4 are effectively summarized as spots on the Hirshfeld surfaces; the large circular depressions (deep red), which are visible on the d_{norm} surfaces, are indicators of hydrogen-bonding contacts. The small area and light colour on the surfaces indicate weaker and longer contacts, contacts other than hydrogen bonds.

(a)



(b)

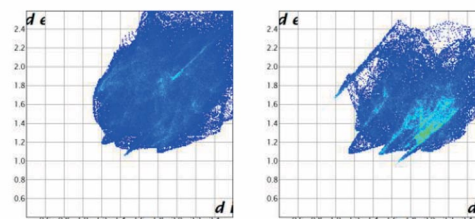


Figure 9. (a) Hirshfeld surfaces of the complex anions in compound **1** (top) and in compound **2** (bottom). (b) 2D fingerprint plots derived from HSs: compound **1** (left) and compound **2** (right).

Table 4. Hydrogen-bond parameters for compound **2**.^[a]

D–H...A	$d(\text{D–H})$ [Å]	$d(\text{H...A})$ [Å]	$d(\text{D...A})$ [Å]	$\angle(\text{DHA})$ [°]
C(24)–H(24)...S(4)#3	0.95	2.82	3.541(12)	133
C(28)–H(28)...N(3)#4	0.95	2.62	3.432(14)	144

[a] Symmetry transformation used to generate equivalent atoms: #3 $x, 1 + y, z$; #4 $1 - x, 1 - y, -z$.

A plot of d_i versus d_e gives a 2D fingerprint plot [Figure 9 (b)], which identifies the occurrence of different kinds of intermolecular interactions. Complementary regions are visible in the fingerprint plots, where one molecule acts as a donor ($d_e > d_i$) and the other as an acceptor ($d_e < d_i$). The N \cdots H close contacts vary from 13.9% in compound **1** to 5.5% in compound **2**. The C \cdots H contacts vary from 20.5% in compound **1** to 15.6% in compound **2**. The S \cdots H weak contacts vary from 21.8% in compound **1** to 8.4% in compound **2** (see Section 8 in the Supporting Information).

Conclusion

We have described the synthesis and characterization of two Ni^{III}-bis(dithiolato) complexes, [Bu₄N][Ni^{III}(6,7-qdt)₂] (**1**) and [Ph₄P][Ni^{III}(Ph₂6,7-qdt)₂] (**2**), that are based on unique dithiolene ligands. Compounds **1** and **2** are additionally characterized by electrochemical and ESR studies, in addition to their unambiguous characterization by single-crystal X-ray structure determination. The described compounds are unique in the sense that they get reduced reversibly at very low potentials. This demonstrates that their respective reduced analogues [Bu₄N]₂[Ni^{II}(6,7-qdt)₂] and [Ph₄P]₂[Ni^{II}(Ph₂6,7-qdt)₂] can act as oxidation catalysts. The title compounds exhibit well-defined electronic absorption bands that have been corroborated with theoretical (DFT) calculations. This is a rare report in which theoretical calculations have been performed on a Ni^{III}-bis(dithiolato) system. The crystal structures of compounds **1** and **2** show interesting supramolecular hydrogen-bonding networks, formed by C–H \cdots S and C–H \cdots N weak contacts. Hirshfeld surfaces (HSs) and 2D fingerprint plots (FPs) corroborate these supramolecular interactions.

Experimental Section

General: All the chemicals for the synthesis were commercially available and used as received. 1,2-Diaminobenzene-bis(thiocyanate) (**A**),^[15] quinoxaline-6,7-dithiol (H₂6,7-qdt; **L**₁),^[7] and [Bu₄N]₂[Ni(6,7-qdt)₂] (**1a**),^[7] diphenylquinoxaline-6,7-dithiol (**L**₂)^[7] and [Ph₄P]₂[Ni(Ph₂6,7-qdt)₂]^[7] were prepared according to literature procedures. Syntheses of metal complexes were performed under N₂ by using standard inert-atmosphere techniques. Solvents were dried by standard procedures. Microanalytical (C, H, N) data were obtained with a FLASH EA 1112 Series CHNS Analyzer. Infrared (IR) spectra were recorded from KBr pellets with a JASCO FT/IR-5300 spectrometer operating in the region 400–4000 cm⁻¹. ¹H NMR spectra of compounds were recorded with a Bruker DRX-400 spectrometer using Si(CH₃)₄ [TMS] as an internal standard. Electronic absorption spectra of solutions and diffuse reflectance spectra of solid compounds were recorded with a UV-3600 Shimadzu UV/Vis/NIR spectrophotometer. A Cypress model CS-1090/CS-1087 electroanalytical system was used for the cyclic voltammetric experiments. The electrochemical experiments were measured in DMF containing [Bu₄N][ClO₄] as a supporting electrolyte, by using a conventional cell consisting of two platinum wires as the working and counter electrodes, and a Ag/AgCl electrode as a reference. The potentials reported here are uncorrected for junction contributions.

[Bu₄N][Ni(6,7-qdt)₂] (1**):** Mono anionic compound **1** was obtained as a brown powder by I₂ oxidation of the corresponding

[Bu₄N]₂[Ni^{II}(6,7-qdt)₂] complex: a solution of I₂ (0.025 g, 0.1 mmol) in CH₃CN (10 mL) was added dropwise to a filtered solution of [Bu₄N]₂[Ni^{II}(6,7-qdt)₂] (0.185 g, 0.2 mmol) in CH₃CN (20 mL) and the mixture was allowed to stir for 2 h at room temperature. The resulting brown precipitate was filtered and washed with a small amount of methanol and hexane. Single crystals, suitable for X-ray diffraction, were grown by slow diffusion of diethyl ether into a CH₃CN solution of the obtained solid, yield 0.115 g (84% based on Ni^{II} complex used). C₃₂H₄₄N₅NiS₄ (685.67): calcd. C 56.05, H 6.47, N 10.21, S 18.71; found C 56.15, H 6.42, N 10.28, S 18.65. IR (KBr): $\tilde{\nu}$ = 3435 (br), 2959 (m), 1440 (w), 1413 (w), 1380 (w), 1172 (m), 1072 (w), 1019 (m), 876 (m), 783 (w), 597 (s), 515 (s) cm⁻¹.

[Ph₄P][Ni(Ph₂6,7-qdt)₂] (2**):** Mono anionic compound **2** was obtained as a dark-brown powder by I₂ oxidation of the corresponding [Ph₄P]₂[Ni^{II}(Ph₂6,7-qdt)₂] complex: a solution of I₂ (0.025 g, 0.1 mmol) in CH₃CN (10 mL) was added dropwise to a filtered solution of [Ph₄P]₂[Ni(Ph₂6,7-qdt)₂] (0.284 g, 0.2 mmol) in CH₃CN (20 mL) and the mixture was allowed to stir for 2 h at room temperature. The resulting dark-brown powder precipitate was filtered and washed with a small amount of MeOH and hexane. Single crystals, suitable for X-ray diffraction, were grown by slow diffusion of diethyl ether into a CHCl₃ solution of the obtained dark-brown powder, yield 0.213 g (88% based on Ni^{II} complex used). C₆₅H₄₅Cl₃N₄NiPS₄ (1206.32): calcd. C 64.71, H 3.76, N 4.64, S 10.63; found C 64.82, H 3.71, N 4.59, S 10.71. IR (KBr): $\tilde{\nu}$ = 3441 (br), 1424 (s), 1336 (w), 1190 (m), 1117 (w), 1080 (s), 1020 (w), 865 (w), 820 (w), 723 (m), 690 (m) cm⁻¹.

X-ray Crystallography: Single crystals, suitable for facile structural determination for the compounds **1** and **2**, were analysed with a three-circle Bruker SMART APEX CCD area detector system under a Mo-*K* α (λ = 0.71073 Å) graphite-monochromatic X-ray beam. The frames were recorded with an ω scan width of 0.3°, each for 10 s, with a crystal–detector distance of 60 mm, collimator 0.5 mm. Data reduction was performed by using SAINTPLUS.^[15] Empirical absorption corrections were made by using equivalent reflections and were performed with the SADABS program.^[16] The structures were solved by direct methods and least-squares refinement on *F*² for both compounds by using SHELXS-97.^[16] All non-hydrogen atoms were refined anisotropically. The hydrogen atoms were included in the structure factor calculation by using a riding model. The crystallographic parameters, data collection and structure refinement of the compounds **1** and **2** are summarized in Table 1. Selected bond lengths and angles for the compounds **1** and **2** are listed in Table 2.

CCDC-1054536 (for **1**) and -1054537 (for **2**) contain the supplementary crystallographic data for this paper. These data can be obtained free of charge from the Cambridge Crystallographic Data Centre via www.ccdc.cam.ac.uk/data_request/cif.

Computation: Computational simulations for the ground-state as well as excited-state electronic structure calculations of the complex anions of compounds **1** and **2** were performed with the help of well-known density functional theory (DFT) by using the GAUSSIAN 09 suite programming package.^[10] It is well known that the DFT can evaluate the ground-state electronic structure of a moiety exactly (especially for bigger molecules, e.g., a coordination complex anion), depending upon the functional used in the procedure. Theoretical calculations throughout the study were done with the hybrid functional B3LYP, which includes Hartree–Fock (HF) exchange as well as DFT exchange correlations. Non-local correlations were accounted for by the Lee, Yang and Parr (LYP) functional. The LanL2DZ basis set was used for Ni; whereas for

other atoms the 6-311G** basis set was used. Relativistic and other effects of the core electrons of the Ni atom have been accounted for by the inbuilt effective core potential (ECP) LanL2 of the LanL2DZ basis set. It should be mentioned that the polarization effect on C, S and N has been taken care of by incorporating five d-type Gaussian polarization functions into the basis set, whereas for H atoms three p-type polarization functions were included. The ground-state electronic structure calculation of the complex anions were performed by using the self-consistent reaction field (SCRf) procedure of the GAUSSIAN 09 programming package,^[10] where solute complex ions are placed in the solvent cavity (DMF). The ground-state anionic complexes were obtained by full geometry optimization followed by frequency calculations. No imaginary frequencies (the lowest ten frequencies of each anionic complex are available in Section 7 of the Supporting Information) were obtained, which ensured that the optimized structure is not situated at any saddle point of the ground-state potential energy surface. Vertical excitations of the optimized structures were performed by employing the TD-B3LYP method^[17] and using the same basis sets and same environment mentioned above. Other details of the computational output are described in the Supporting Information, Figure S7.

Supporting Information (see footnote on the first page of this article): HRMS spectra, computational outputs, 2D fingerprint plot derived from Hirshfeld surfaces, cyclic voltammograms, hydrogen-bonding interactions in the crystal structure of compound **1** and bond valence sum calculations for nickel in compounds **1** and **2**.

Acknowledgments

The authors thank the Council of Scientific and Industrial Research (CSIR), Government of India [project number 01 (2556)/12/EMR-II] for financial support. The single-crystal X-ray diffraction facility at the University of Hyderabad by the Department of Science and technology (DST), New Delhi is highly acknowledged. The authors thank Mr. Suresh for helping us in the different stages of preparing the manuscript and Mr. Kumar for recording the ESR spectra. Our special thanks go to Professor S. Mahapatra, School of Chemistry and University of Hyderabad, for his help with the theoretical calculations and to the CMSD for computational facilities.

- [1] a) R. Kato, *Chem. Rev.* **2004**, *104*, 5319–5346; b) X. M. Ren, S. Nishihara, T. Akutagawa, S. Noro, T. Nakamura, *Inorg. Chem.* **2006**, *45*, 2229–2234; c) M. L. Mercuri, P. Deplano, L. Pilia, A. Serpe, F. Artizzu, *Coord. Chem. Rev.* **2010**, *254*, 1419–1433; d) A. T. Coomber, D. Beljonne, R. H. Friend, J. L. Brédas, A. Charlton, N. Robertson, A. E. Underhill, M. Kurmoo, P. Day, *Nature* **1996**, *380*, 144–146; e) N. Robertson, L. Cronin, *Coord. Chem. Rev.* **2002**, *227*, 93–127.
- [2] a) L. Serrano-Andrés, A. Avramopoulos, J. Li, P. Labéguerie, D. Bégue, V. Kellö, M. G. Papadopoulos, *J. Chem. Phys.* **2009**, *131*, 134312–134322; b) P. Deplano, L. Pilia, D. Espa, M. L. Mercuri, A. Serpe, *Coord. Chem. Rev.* **2010**, *254*, 1434–1447; c) C.-T. Chen, S.-Y. Liao, K.-J. Lin, L.-L. Lai, *Adv. Mater.* **1998**, *3*, 334–338.
- [3] a) U. T. Mueller-Westerhoff, B. Vance, D. I. Yoon, *Tetrahedron* **1991**, *47*, 909–932; b) J.-F. Bai, J.-L. Zuo, W.-L. Tan, W. Ji, Z. Shen, H.-K. Fun, K. Chinnakali, I. A. Razak, X.-Z. You, C. M. Che, *J. Mater. Chem.* **1999**, *9*, 2419–2423; c) P. Deplano, M. L. Mercuri, G. Pintus, E. F. Trogu, *Comments Inorg. Chem.* **2001**, *22*, 353–374; d) M. C. Aragoni, M. Arca, T. Cassano, C. Denotti, F. A. Devillanova, R. Frau, F. Isaia, F. Lelj, V. Lippolis, L. Nitti, P. Romaniello, R. Tommasi, G. Verani, *Eur. J. Inorg. Chem.* **2003**, 1939–1947; e) S. I. G. Dias, S. Rabaca, I. C. Santos, L. C. J. Pereira, R. T. Henriques, M. Almeida, *Inorg. Chem. Commun.* **2012**, *15*, 102–105; f) P. Basu, A. Nigam, B. Mogesa, S. Denti, V. N. Nemykin, *Inorg. Chim. Acta* **2010**, *363*, 2857–2864.
- [4] K. D. Karlin, E. I. Stiefel, *Progress in Inorganic Chemistry*, vol. 52: *Dithiolene Chemistry: Synthesis Properties, and Applications*, John Wiley, New York, **2004**.
- [5] a) V. Madhu, S. K. Das, *Cryst. Growth Des.* **2014**, *14*, 2343–2356; b) V. Madhu, S. K. Das, *Dalton Trans.* **2011**, *40*, 12901–12908; c) V. Madhu, S. K. Das, *J. Chem. Sci.* **2006**, *118*, 611–617; d) V. Madhu, S. K. Das, *Polyhedron* **2004**, *23*, 1235–1242; e) R. Bolligarla, G. Durgaprasad, S. K. Das, *Inorg. Chem. Commun.* **2011**, *14*, 809–813; f) R. Bolligarla, S. K. Das, *CrystEngComm* **2010**, *12*, 3409–3412; g) X. Ribas, J. Dias, J. Morgado, K. Wurst, M. Almeida, J. Veciana, C. Rovira, *CrystEngComm* **2002**, *4*, 564–567.
- [6] a) G. Durgaprasad, S. K. Das, *J. Chem. Sci.* **2015**, *127*, 295–305; b) G. Durgaprasad, R. Bolligarla, S. K. Das, *J. Organomet. Chem.* **2011**, *696*, 3097–3105; c) G. Durgaprasad, R. Bolligarla, S. K. Das, *J. Organomet. Chem.* **2012**, *706*, 37–45; d) G. Durgaprasad, S. K. Das, *J. Organomet. Chem.* **2012**, *717*, 29–40; e) N. M. F. S. A. Cerqueira, B. Pakhira, S. Sarkar, *J. Biol. Inorg. Chem.* **2015**, *20*, 323–335; f) B. K. Maiti, L. B. Maia, K. Pal, B. Pakhira, T. Aviles, I. Moura, S. R. Pauleta, J. L. Nunez, A. C. Rizzi, C. D. Brondino, S. Sarkar, J. J. G. Moura, *Inorg. Chem.* **2014**, *53*, 12799–12808.
- [7] R. Bolligarla, S. N. Reddy, G. Durgaprasad, V. Sreenivasulu, S. K. Das, *Inorg. Chem.* **2013**, *52*, 66–76.
- [8] C.-M. Lee, Y.-L. Chuang, C.-Y. Chiang, G.-H. Lee, W.-F. Liaw, *Inorg. Chem.* **2006**, *45*, 10895–10904.
- [9] B. Zheng, F. Tang, J. Luo, J. W. Schultz, N. P. Rath, L. M. Mirica, *J. Am. Chem. Soc.* **2014**, *136*, 6499–6504.
- [10] M. J. Frisch, G. W. Trucks, H. B. Schlegel, G. E. Scuseria, M. A. Robb, J. R. Cheeseman, G. Scalmani, V. Barone, B. Mennucci, G. A. Petersson, H. Nakatsuji, M. Caricato, X. Li, H. P. Hratchian, A. F. Izmaylov, J. Bloino, G. Zheng, J. L. Sonnenberg, M. Hada, M. Ehara, K. Toyota, R. Fukuda, J. Hasegawa, M. Ishida, T. Nakajima, Y. Honda, O. Kitao, H. Nakai, T. Vreven, J. A. Montgomery Jr., J. E. Peralta, F. Ogliaro, M. Bearpark, J. J. Heyd, E. Brothers, K. N. Kudin, V. N. Staroverov, R. Kobayashi, J. Normand, K. Raghavachari, A. Rendell, J. C. Burant, S. S. Iyengar, J. Tomasi, M. Cossi, N. Rega, J. M. Millam, M. Klene, J. E. Knox, J. B. Cross, V. Bakken, C. Adamo, J. Jaramillo, R. Gomperts, R. E. Stratmann, O. Yazyev, A. J. Austin, R. Cammi, C. Pomelli, J. W. Ochterski, R. L. Martin, K. Morokuma, V. G. Zakrzewski, G. A. Voth, P. Salvador, J. J. Dannenberg, S. Dapprich, A. D. Daniels, Ö. Farkas, J. B. Foresman, J. V. Ortiz, J. Cioslowski, D. J. Fox, *Gaussian 09*, revision C.01, Gaussian, Inc., Wallingford CT, **2010**.
- [11] V. Madhu, S. K. Das, *Inorg. Chem.* **2008**, *47*, 5055–5070.
- [12] D.-Y. Noh, M.-J. Kang, H.-J. Lee, J.-H. Kim, J.-H. Choy, *Bull. Korean Chem. Soc.* **1996**, *17*, 46–50.
- [13] S. K. Wolff, D. J. Grimwood, J. J. McKinnon, M. J. Turner, D. Jayatilaka, M. A. Spackmann, *CrystalExplorer 3.1* (**2013**), University of Western Australia, Crawley, Western Australia, **2005–2013**, <http://hirshfeldsurface.net>.
- [14] a) J. J. McKinnon, D. Jayatilaka, M. A. Spackman, *Chem. Commun.* **2007**, 3814–3816; b) F. L. Hirshfeld, *Theor. Chim. Acta* **1977**, *44*, 129–138; c) M. A. Spackman, D. Jayatilaka, *CrystEngComm* **2009**, *11*, 19–32.
- [15] J. L. Brusso, O. P. Clements, R. C. Haddon, M. E. Itkis, A. A. Leitch, R. T. Okely, R. W. Reed, J. F. Richardson, *J. Am. Chem. Soc.* **2004**, *126*, 8256–8265.
- [16] Bruker AXS Inc., *SADABS, SMART, SAINT and SHELXTL*, Madison, Wisconsin, USA, **2000**.
- [17] U. Salzner, *J. Chem. Theory Comput.* **2013**, *9*, 4064–4073.

Received: July 6, 2015

Published Online: November 4, 2015